MSDE

PAPER

Cite this: *Mol. Syst. Des. Eng.*, 2020, **5**, 820

Competitive hydrogen bonding in supramolecular polymerizations of tribenzylbenzene-1,3,5-tricarboxamides†

Mathijs F. J. Mabesoone, ‡[a] Sinan Kardas, ‡[ab] Héctor Soria-Carrera, [c] Joaquín Barberá, [c] Jesús M. de la Fuente,[c] Anja R. A. Palmans, *[a] Mathieu Fosséprè, [b] Mathieu Surin *[b] and Rafael Martín-Rapún *[cd]

Received 19th March 2020,
Accepted 16th April 2020

DOI: 10.1039/d0me00030b

rsc.li/molecular-engineering

Despite numerous reports on nucleated supramolecular polymerization, the molecular origin of the properties of these supramolecular polymers remains overlooked. Here, the formation of fibers formed by self-assembly of *N*,*N*′,*N*″-tris(alkoxybenzyl)benzene-1,3,5-tricarboxamides (benzyl-BTAs) has been studied using both simulations and experimental techniques. The simulations show that the fibers exhibit a dynamic behavior with stacking defects that appear and propagate differently depending on the BTA molecular structure. To validate theoretical results, a library of eight benzyl-BTAs has been synthesized to compare their supramolecular polymerizations both in the bulk and in apolar solvents. We show that the molecular organization of monomers and dynamics of supramolecular polymers strongly depend on the number and position of the alkoxy substituents on peripheral phenyl rings. By combining theoretical results with experimental measurements, we elucidate the likely role of competitive hydrogen bonding between the central amides and peripheral ether moieties on the stacking behavior of BTAs and the dynamics of structural defects in supramolecular polymers. Our findings open up new design rules for these dynamic materials.

Design, System, Application

Despite the numerous reports on supramolecular polymers, structure–property relationships are still lacking. Here, we designed several new types of substituted tribenzylbenzene-1,3,5-tricarboxamides, as monomers for supramolecular polymerization. To arrive at a rational translation of molecular properties to material properties, we first study the supramolecular polymers with molecular dynamics (MD) simulations. These simulations show that introduction of ether moieties at the monomer periphery induces defects in the polymers, as a result of hydrogen bonding between these ethers and the central amides. The structural defects of the polymers are experimentally confirmed both in bulk and in solution. We anticipate that the rational design rules obtained through our combined computational and experimental insights may facilitate the design of complex and adaptive supramolecular polymers.

1 Introduction

To accelerate the application of supramolecular polymerizations in soft materials, control over the molecular organization is of paramount importance.[1] Material properties, such as conductivity and processability, are indeed dependent on the molecular structure of the monomers.[2,3] Unfortunately, prediction of the structure and stability of a supramolecular polymer remains challenging. Pathway complexity,[4] multiple polymer states[5–7] or kinetic trapping[8] pose significant challenges in rational design of material properties from monomer structures. Despite the challenges posed by these facets of supramolecular polymerizations, the competition between several polymerization pathways has given rise to promising systems, such as living supramolecular polymers,[9–11] thermally bisignate polymerizations[12,13] and kinetically trapped states.[14,15]

Understanding of complex supramolecular polymerizations has been helped with computational approaches. The development of numerical models by among

[a] *Laboratory of Macromolecular and Organic Chemistry and Institute for Complex Molecular Systems, Eindhoven University of Technology, Eindhoven, The Netherlands. E-mail: A.Palmans@tue.nl*
[b] *Laboratory for Chemistry of Novel Materials, Center of Innovation and Research in Materials and Polymers, University of Mons–UMONS, Belgium. E-mail: Mathieu.Surin@umons.ac.be*
[c] *Departamento de Química Orgánica – Instituto de Ciencia de Materiales de Aragón, Universidad de Zaragoza-CSIC, Zaragoza, Spain. E-mail: rmartin@unizar.es*
[d] *Instituto de Nanociencia de Aragón, Universidad de Zaragoza, Zaragoza, Spain*
† Electronic supplementary information (ESI) available: Supporting information for this article is given *via* a link at the end of the document. See DOI: 10.1039/d0me00030b
‡ These authors contributed equally.

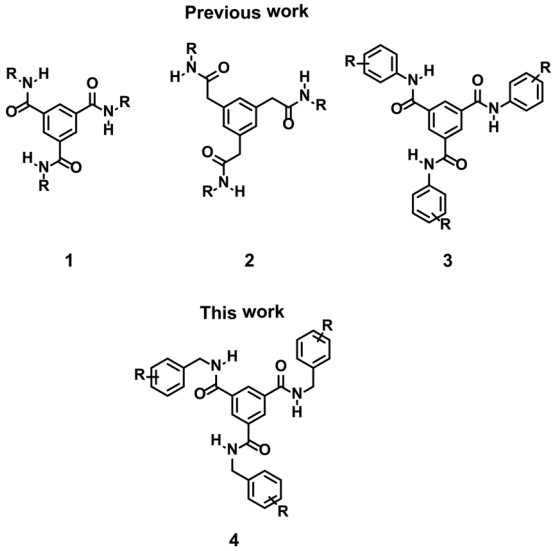

Scheme 1 Chemical structures of previously studied BTAs **1**–**3** and the BTA **4** studied in this work.

others van der Schoot,[16,17] ten Eikelder and Markvoort,[18–20] and Würthner[21,22] has given great insights into the thermodynamic properties of these supramolecular systems and provided rationales for some of their counterintuitive behavior.[23,24] In addition, MD simulations have given unrivalled atomistic insights into the network of interactions in supramolecular polymers in organic solvents[25–29] and hydrophobically collapsed structures in aqueous media.[30–32] Interestingly, dynamics of defects along the self-assembled BTA fibers have been pointed out thanks to the atomistic information coming from MD simulations.[33] These simulations enable a correlation of molecular features to the macroscopic properties of the materials. However, approaches that correlate microscopic insights from simulations with experimentally obtained material properties to arrive at general structure–property relationships are not commonplace.

To gain further insights into the way hydrogen bonding affects the structure and dynamics of supramolecular polymers, an efficient strategy would be to guide the design of supramolecular systems by systematic molecular modelling techniques. The factors that direct self-assembly and dynamics of supramolecular systems could thus be highlighted to propose structure–property relationships.

In the past, we and others have studied in detail the self-assembly properties of benzene-1,3,5-tricarboxamides (BTAs) **1** and of methylene bridged analogues **2** (Scheme 1) by a combination of experimental and computational studies. Computational studies on **1** have shed light on the molecular principles underlying its strongly cooperative supramolecular polymerization.[25,34,35] Combined experimental and computational studies have revealed furthermore a subtle influence of the solvent on the geometry and stability of the supramolecular polymers of **1**.[36]

In contrast, when a methylene spacer is installed between the central benzene core and the amides in the conformationally flexible derivative **2**, a strong dependency on solvent structure has been observed.[28] Using a computational approach, this strong solvent dependency could be attributed to subtle differences in stabilization of various amide conformations. In a third structural variation, the addition of a phenyl ring between the soluble alkyl chains and the amide (derivative **3**) resulted in a complete loss of aggregation, presumably due to the loss in intermolecular hydrogen-bond formation.[37] The understanding of the molecular dynamics and how this impacts the experimentally observed behavior of BTA derivatives **1**–**3** prompted us to design a library of more conformationally flexible benzyl-BTA derivatives, **4**. Due to the methylene group between the central amides and peripheral phenyl group, derivatives of **4** were anticipated to be more prone to form intermolecular hydrogen bonds than **3** and therefore more likely to cooperatively self-assemble. The different effects of the number and position of the alkoxy groups on the phenyl rings have been observed before but are not well understood for supramolecular polymerizations.[38–41] We systematically varied the position and number of alkoxy groups on the peripheral phenyl ring (Scheme 2) to obtain a more detailed understanding of the effect of these substitution patterns on the supramolecular structure. To permit the use of circular dichroism (CD) spectroscopy, which is a sensitive tool to assess the cooperativity and stability of supramolecular polymerizations, all substitution patterns have one representative comprising chiral, non-racemic (*S*)-3,7-dimethyloct-1-yl side chains (**Cit-3**, **Cit-6**, **Cit-9** and **Sym-Cit-6**).

Here, we put forward a comprehensive approach to relate the molecular structures to their self-assembly behavior, by starting from MD simulations and subsequently analyzing the systems experimentally. Our results show that the combined computational and experimental approach can elucidate counterintuitive, competitive hydrogen bonding patterns between the central amides and peripheral ethers, which considerably impact the stability of supramolecular polymers. These structure–property relationships may provide important guidelines towards a rational design of functional supramolecular polymers.

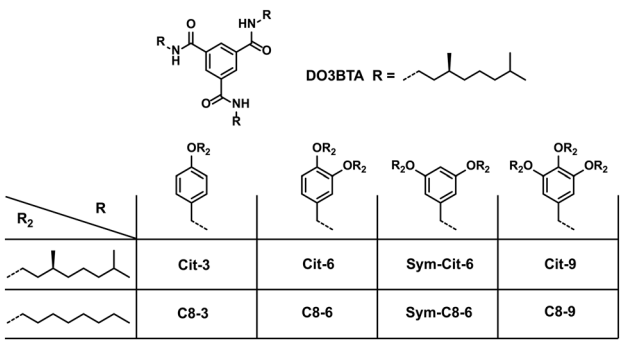

Scheme 2 Library of chiral and achiral alkoxybenzyl-substituted BTAs studied in this work.

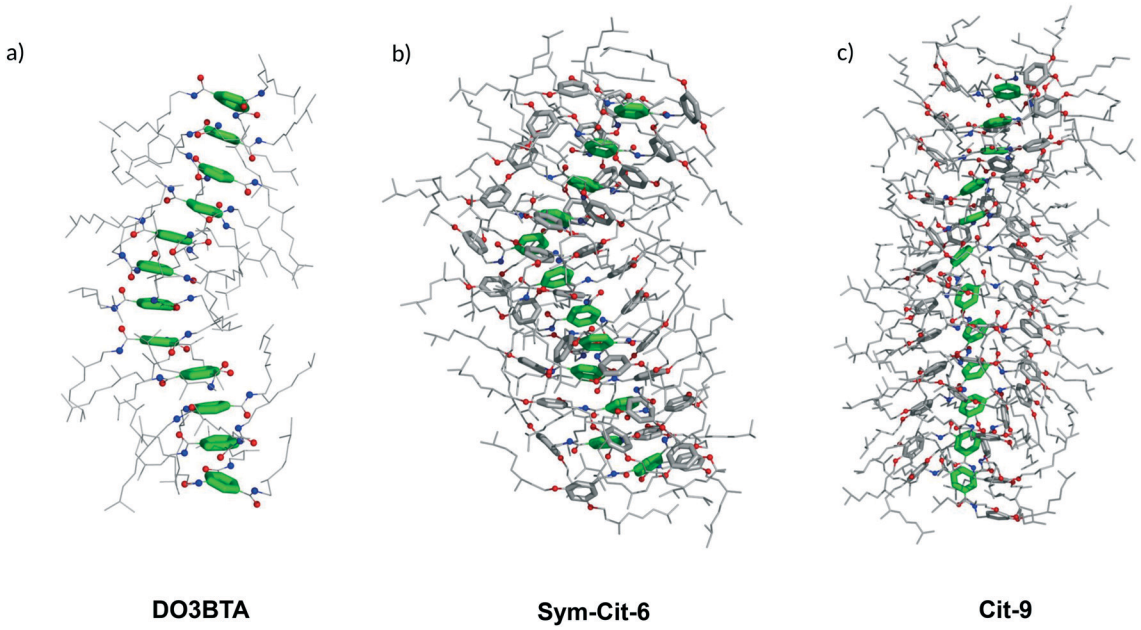

Fig. 1 Snapshots extracted in the early steps of the MD simulations (taken at 1 ns) of 12-unit long fibers of **DO3BTA** (a), **Sym-Cit-6** (b) and **Cit-9** (c), showing the helical organization of the BTA cores (green sticks) and the interdigitation of the side chains (grey sticks for benzyl groups and grey lines for alkoxy chains). Oxygen and nitrogen atoms are depicted in red and blue, respectively.

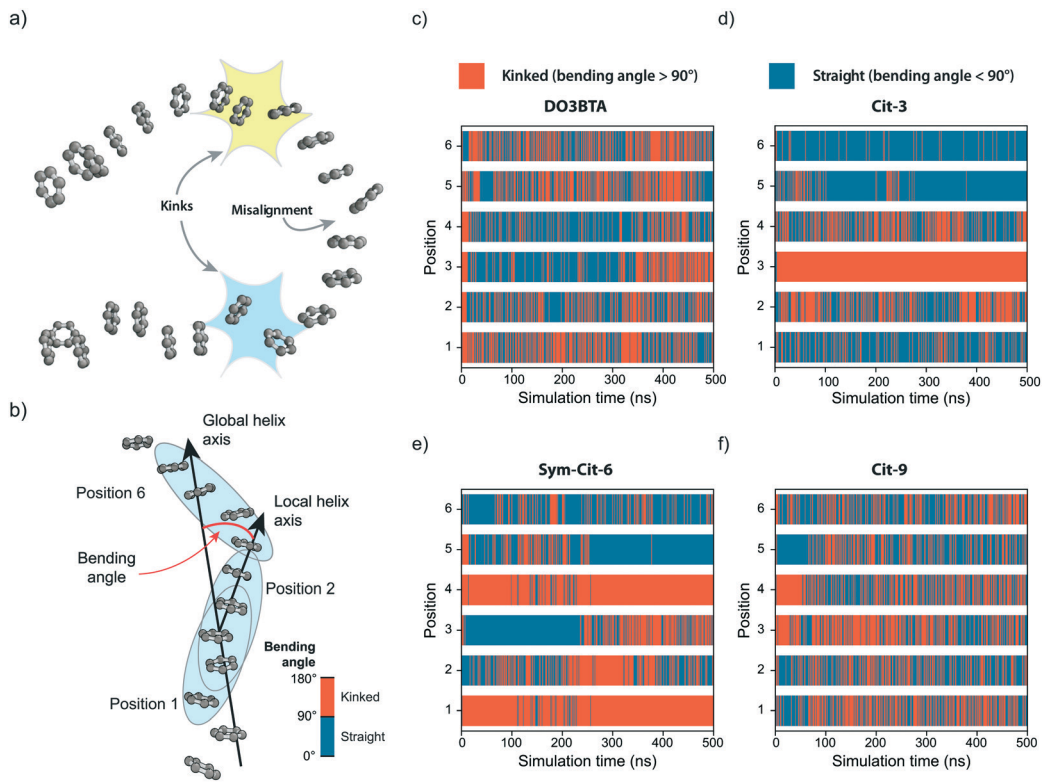

Fig. 2 a) Snapshot of the MD simulation of the 24 units long fiber of **Sym-Cit-6** at 250 ns showing the presence of structural defects (minor misalignment, clear kink). Only the benzene cores are shown for clarity. b) The HELANAL-Plus software defines a global helix axis by fitting a helix to the entire fiber of BTAs. Similarly a local helix axis is defined for each position of a sliding window of four consecutive BTA cores, of which examples are indicated by the position markers. The bending angle corresponds to the angle between the global and local helix axes. The energy-minimized structure of BTA cores of the 12 units long fiber of **Sym-Cit-6** is shown. c–f) Evolution of the local bending angles for the 6 positions, as indicated in Fig. 2b, as obtained from the HELANAL-Plus analysis over the course of the 500 ns MD simulation for **DO3BTA** (c), **Cit-3** (d), **Sym-Cit-6** (e) and **Cit-9** (f). Kinked regions appear through a binary color code of bending angles (BA): blue regions indicate straight sections of the fiber (BA $< 90°$), while red regions indicate kinked sections (BA $> 90°$).

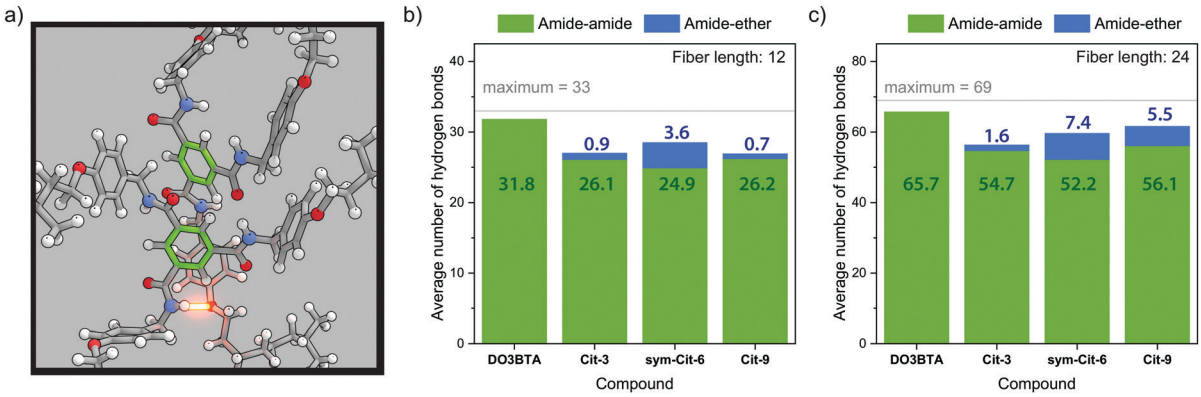

Fig. 3 a) Cartoon representation of the **Cit-3** simulation with 24 units at 40 ns, showing the highlighted amide–ether hydrogen bond. The aromatic cores of the two benzyl-BTAs are highlighted in green. b and c) The number of amide–amide and amide–ether H-bonds averaged over the entire simulation for fibers of 12 BTAs (b) and 24 BTAs (c).

2 Results and discussion

Molecular dynamics simulations of benzyl-BTAs show competitive hydrogen bonding

MD simulations were carried out to evaluate the influence of lateral groups and fiber length on the supramolecular assembly and dynamics of benzyl-BTA fibers. To do so, we compared a model BTA-based compound, **DO3BTA**, with the series of compounds designed in this study (Scheme 2). BTA and benzyl-BTA fibers of 12- and 24-units long were built with an intercore distance between BTAs of 5 Å. Their geometries were initially optimized by energy-minimization, to be used as starting structures for MD simulations on a 500 ns timescale. In the early steps of the MD simulations, the intercore distances drop to 3.4 Å and the cores rotate relative to each other due to π-stacking and hydrogen bonding between BTA monomers. The fibers become helical and organize in short ordered segments of stacked BTAs with structural defects between these segments (see snapshots in Fig. 1). These defects consist of minor misalignments and clear kinks that propagate along the MD simulations (Fig. 2a). Each ordered segment is made of several BTAs and characterized by intercore distances of around 3.4 Å. For alkoxybenzyl-BTA derivatives, some peripheral phenyl rings are π-stacked in dimers, while alkoxy side chains protrude from the helical fibers and interdigitate between adjacent BTA units along a single fiber (Fig. 1). The defects in the fibers are characterized by a large distance (>4 Å) between centers of mass of pairs of adjacent BTAs (Fig. S1†) and small angles (well below 180°) between the centers of mass of three consecutive BTAs (Fig. S2†). A cartoon representation of the particularly disordered **Sym-Cit-6** fiber of 24 units is given in Fig. 2a.

The kinks observed in the simulations are localized in sections of the fibers with large bending angle compared to the helix axis (Fig. 2b), as estimated with the helical analysis software HELANAL-Plus[42] (see computational details in the ESI† for the details). The results of these analyses (Fig. 2c–f and S3 and S4†) show two types of information: a sequential information (*Y* axis, where does the kink appear in the fiber?), and a temporal information (*X* axis, when does the kink appear during the simulation?). Interestingly, the number of persistent kinks depends on the monomer structure. For the **DO3BTA** model compound, there is a random alternation between straight sections (Fig. 2c, ordered segments in dark blue) and kinked sections (Fig. 2c, structural defects in red) along the fiber. The kinked and straight sections are interchanging on a timescale ranging from a few ns to tens of ns. Remarkably, the introduction of the alkoxy moieties in the benzyl-BTA derivatives appears to introduce clear structural defects in the fibers. In

Table 1 NH-Stretch and CO-stretch frequencies [cm^{-1}] obtained from bulk IR measurements and transition temperatures [°C] and corresponding enthalpies [kJ mol^{-1}] of BTAs obtained by DSC measurements[a]

Compound[a]	$\nu_{NH\text{-}stretch}$ (cm^{-1})	$\nu_{CO\text{-}stretch}$ (cm^{-1})	Thermal behavior
Cit-3	3231	1637	C 62 (1.7) Col_{ho} 182 (8.8) I
C8-3	3244	1638	C 123 (13.3) Col_{ro} 185 (15.6) I
Cit-6	3237	1636	Col_{ho} 133 (17.3) I
C8-6	3262	1647	C 55 (9.2) Col_{ho} 151 (16.0) I
Sym-Cit-6	3331	1667	I
Sym-C8-6	3329	1664	g 23 I
Cit-9	3317	1662	I
C8-9	3230	1649	Col_{ho} 88 (10.0) I

[a] All DSC data derived from the second heating run. g = isotropic glass. C = crystalline phase; Col_{ro} = rectangularly ordered columnar phase; Col_{ho} = hexagonally ordered columnar phase; I = isotropic phase.

Table 2 IR frequencies [cm^{-1}] of the NH-stretch and CO-stretch vibrations of the BTAs obtained in 250 μM MCH and $CHCl_3$ solutions. Full spectra are given in Fig. S8–S11

	$\nu_{NH\text{-stretch}}$ (cm^{-1})		$\nu_{CO\text{-stretch}}$ (cm^{-1})	
Compound	MCH	$CHCl_3$	MCH	$CHCl_3$
Cit-3	3229	3448	1640	1666
Cit-9	3315	3447	1665	1666
C8-9	3322	3447	1666	1666
Cit-6	3326	3443	1663	1663
C8-6	3318	3445	1664	1663
Sym-Cit-6	3321	3445	1667	1665
Sym-C8-6	3331	3445	1666	1666

contrast to fibers of **DO3BTA**, fibers of **Cit-3** and **Sym-Cit-6** (Fig. 2d and e) show relatively short straight (dark blue) sections separated by persistent kinks (red continuous lines) in the middle of the fiber and at positions 1 and 4, respectively. Fibers of **Cit-9** (Fig. 2f), which have the highest degree of alkoxy substitution on the peripheral phenyl rings, do not show any persistent kinks. Similar, yet less pronounced results are obtained in the simulations of the supramolecular polymers composed of 24 units of benzyl-BTAs (Fig. S4†).

The results obtained from the HELANAL-Plus analysis show that the steric hindrance imposed by a high number of alkoxy groups on the peripheral phenyl rings of **Cit-9** reduces the possibility of fibers to kink. This different behavior likely arises from the larger steric hindrance between adjacent chiral alkoxy side chains in **Cit-9** compared to the **Sym-Cit-6** and **Cit-3**. In the case of **Cit-9**, the possibility of the benzyl-BTA units to tilt out of the columnar axis is reduced, resulting in dynamic, but relatively ordered supramolecular polymers.

The striking difference between the structural dynamics of the defects is encoded into the structure of the benzyl-BTAs. To investigate the origin of kinks in the fibers, we examined persistent hydrogen bonds which are present at least 90% of the MD time. Fig. 3 reports the number of hydrogen bonds in the different BTA fibers averaged over the entire MD simulation. The fibers of **DO3BTA** possess the highest number of hydrogen bonds: around 32 hydrogen bonds of the maximum of 33 hydrogen bonds in a fiber of 12 BTA units. Fibers of benzyl-BTAs with the alkoxybenzyl periphery tend to have less amide–amide hydrogen bonds. Rather unexpectedly, however, a considerable number of hydrogen bonds between the central amides and the peripheral ether moieties were observed. These hydrogen bonds, which have an average length of approximately 3.3 Å, are slightly longer than the amide–amide hydrogen bonds, which have an average length of 3.1 Å, which is typical for such hydrogen bonds.[32]

The amide–ether hydrogen bonds are persistently present at kink sites (*vide supra*), where a fraction of the amide–amide hydrogen bonds is broken (Fig. 3a and S5†). Although a small number of non-persistent amide–ether hydrogen bonds may also be present in straight portions of the fibers, the strong correlation between the amide–ether hydrogen bond and a structural defect strongly suggests kinking of the fiber is related to the amide–ether hydrogen bond.

The presence of the amide–ether hydrogen bonds in the benzyl-BTAs can explain the above described differences in dynamic behavior between the various compounds. When going from polymers of **Cit-3** to **Sym-Cit-6**, the number of amide–ether hydrogen bonds increases as the peripheral phenyl rings have more alkoxy substituents which are, in addition, better positioned to interact with the amide groups at the central phenyl ring. This higher number of amide–ether hydrogen bonds correlates with the higher number of defects in **Sym-Cit-6** polymers. In contrast, fibers of **Cit-9**, which possess the highest number of alkoxy side chains, yet the lowest number of defects, concomitantly show the lowest number of amide–ether hydrogen bonds. Interestingly, this difference is less pronounced in the results obtained for **Cit-9** polymers of 24 units (Fig. 3c), where the average of 5.5 amide–ether intermolecular hydrogen bonds is much higher than the double value obtained for a fiber of 12 units (2 × 0.7 in average). In other words, in the 24 units long fiber of **Cit-9**, amide–ether intermolecular hydrogen bonds occur at a higher extent, but there are still less of these competitive hydrogen bonds than in case of **Sym-Cit-6**.

Analysis of the MD results indicates that an increasing number of alkoxy substituents that are well-positioned on peripheral phenyl rings increases the number of defects in the fibers as a consequence of competitive amide–ether hydrogen bonds becoming more likely. However, for the

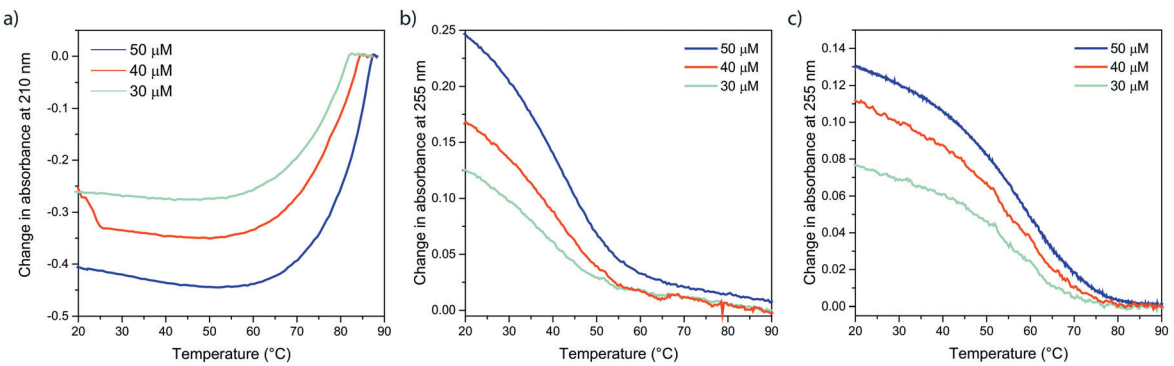

Fig. 4 VT-CD results obtained for **Cit-3** (a), **Cit-9** (b) and **C8-9** (c) at various concentrations in MCH.

fibers of **Cit-9**, which possess three alkoxy chains per benzyl group, the formation of amide–ether hydrogen bonds is counterbalanced, possibly due to additional steric effects which reduce the possibility of the fiber to kink. All in all, the number of solubilizing alkoxy chain in the periphery of benzyl-BTAs need to be considered in the design of molecules as they induce competitive hydrogen-bonding interactions into the system. Using these computationally derived design rules, the stability of the supramolecular polymers can be controlled, as our experimental results show in the next section.

Experimental studies confirm computationally observed trends

To test whether MD simulations accurately predict the different degrees of ordering for the different compounds, the eight benzyl-BTA derivatives were extensively studied both in the bulk and in solution. All benzyl-BTAs were synthesized according to the procedures described in the Schemes S1–S4 in the ESI† and obtained in excellent purity (full characterization in the ESI†).

The results obtained for **Cit-3** clearly show that the *para*-alkoxy substituted derivatives form supramolecular polymers both in the bulk as well as in solution. Similarly to alkyl-BTAs, **Cit-3** and **C8-3** are thermotropic liquid crystals.[43] Polarized optical microscopy (POM) results show that **Cit-3** and **C8-3** exhibit a pseudo-focal conic texture upon slow cooling from the isotropic liquid, indicating the presence of a columnar liquid crystal phase (Fig. S6†). X-ray diffraction (XRD) measurements allow us to confirm the ordered columnar phases, with an interdisc distance of 3.5 Å as was previously reported for alkyl-BTAs (Table S1†).[44]

The enthalpies associated to the mesophase to isotropic liquid transitions, 8.8 and 15.6 kJ mol^{-1}, are similar to those observed for alkyl-BTAs (12–17 kJ mol^{-1}).[43] This similarity indicates that the structure of the mesophases could be equivalent, and consist of a 2D packing of one dimensional fibers, which are each stabilized through helical arrays of threefold hydrogen bonding.[44]

The IR spectra in the bulk provide further support for the presence of a threefold hydrogen-bonded helical array, with NH-stretch and CO-vibrations around 3240 and 1640 cm^{-1} respectively. The vibrations at those wavenumbers are very indicative of the formation of strong, triple helical hydrogen bonds (Table 1). The same absorption bands are observed for **Cit-3** in methylcyclohexane (MCH) solution showing that the one-dimensional fibers are stable in MCH and possess a similar structure as observed in the bulk. The results in chloroform ($CHCl_3$) solutions show a shift of the NH and CO stretch vibrations to higher wavenumbers (Table 2), indicating that in $CHCl_3$, the hydrogen bonds are disrupted. Interestingly, the high degree of ordering that is enabled by the aliphatic side chain of **C8-3** renders this compound insoluble in MCH. Since the insolubility impairs further detailed analysis of the structures in solution, we decided not to further investigate this compound.

The strong hydrogen bonding and highly ordered columnar packing in the supramolecular polymers of **Cit-3**, as observed in the IR results, is further illustrated in the variable temperature CD (VT-CD) and variable temperature UV (VT-UV) experiments (Fig. 4a and S12†). At temperatures above 87 °C, **Cit-3** is molecularly dissolved in 50 μM solutions in MCH. Upon cooling the solutions below this temperature, a sharp onset of the CD signal is observed, indicating that ordered supramolecular polymers are formed *via* a very cooperative process. By fitting the cooling curves of three different concentrations simultaneously to a thermodynamic mass-balance model of a nucleated supramolecular polymerization (Fig. S18†), we determined the enthalpy of elongation and nucleation of **Cit-3** at −71 kJ mol^{-1} and −54 kJ mol^{-1}, the entropy of elongation at −117 J mol^{-1} K^{-1} and the cooperativity parameter, σ, at 293 K at 9.3×10^{-4}. The cooperativity in the supramolecular polymerization of **Cit-3** is in good agreement with the presence of intermolecular hydrogen bonding in solution as shown by IR measurements.[45,46]

C8-9 and **Cit-9** exhibit a different behavior from **C8-3** and **Cit-3**. Although **C8-9** is a liquid crystal at room temperature, its clearing point is 94 K lower than the clearing point of **C8-3**, as generally occurs upon increasing the number of flexible alkyl chains in the periphery of discotic molecules. The mesophase can be assigned as ordered columnar hexagonal based on the weakly birefringent pseudo-focal conic texture by POM, and the X-ray diffraction pattern (Table S1†). Branching in the alkyl chains further destabilizes the mesophase for **Cit-9**, which is an isotropic liquid. Consistently, IR measurements in the bulk show the formation of supramolecular polymers in bulk for **C8-9**, as indicated by the NH and CO stretch vibrations around 3240 and 1650 cm^{-1}, but not for **Cit-9** (Table 1). If present, the amide–amide intermolecular hydrogen bonds are even weaker in solution as shown by the NH and CO stretch vibrations around 3320 and 1665 cm^{-1} even for **C8-9** in MCH (Table 2).

In line with the observations made in bulk and concentrated solutions, VT-CD and UV experiments of **Cit-9** and VT-UV **C8-9**, where the wavelength of maximum CD intensity of **Cit-9** is followed, indicate that supramolecular polymers are formed only in a weakly cooperative manner (Fig. 4b and c and S13 and S18†). By fitting the data to the model, the enthalpy and entropy of elongation of **Cit-9** are determined at −72 kJ mol^{-1} and −144 J mol^{-1} K^{-1} and at −61 kJ mol^{-1} and −100 J mol^{-1} K^{-1} for **C8-9**. The cooperativity parameter, σ, of both compounds is determined at 0.04 and 0.03, respectively, at 293 K. The larger entropic penalty of polymerization of **Cit-9** presumably reflects the loss of entropy resulting from the organization of the larger number of alkoxy chains, while the higher value of σ suggests that polymers of **Cit-9** are shorter than the polymers of **Cit-3** under similar conditions.[47] Similar observations on the effect of cooperativity and stability on peripheral substitution patterns in BTA derivatives has also been observed in related compounds.[41]

Sym-Cit-6 and **Sym-C8-6**, which were obtained as viscous liquids, did not show signs of hydrogen bonding either in bulk or in MCH solutions as shown by the wavenumbers of the NH and CO stretch vibrations (Tables 1 and 2). Accordingly, the compounds were isotropic under POM and no transitions could be observed by DSC or by VT-UV and CD (Fig. S14 and S16†). Liquid crystallinity has been rarely reported for discotic compounds with a 3,5-substitution pattern compared to 3,4,5- or 3,4-substitution patterns.[48] Therefore, we also synthesized the 3,4-disubstituted analogues **Cit-6** and **C8-6**. For those compounds, POM shows a clear pseudo-focal conic texture at high temperatures, indicating the presence of a columnar liquid crystal phase. The isotropization temperature is lower than for **C8-3** and **Cit-3** but higher than for **C8-9** and **Cit-9**, showing that the mesophase is intermediate in stability. However, the transition enthalpy is similar to **C8-3** and to alkyl-BTAs, suggesting the structure of the mesophase could be also the same. Indeed, the mesophase can be assigned as ordered columnar hexagonal based on XRD measurements on shear aligned samples (Fig. S7†). First, a set of equatorial reflections is observed in the small angle region with spacings in the reciprocal ratio $1:\sqrt{7}:\sqrt{12}$, compatible with a 2D hexagonal lattice. Second, a sharp arc is centered on the meridian and corresponds to 3.5 Å, which is the typical stacking distance in ordered columnar mesophases. The diffuse halo that results from the aliphatic tails shows a four-spot pattern as previously reported for alkyl-BTAs.[44]

Consistently, strong hydrogen bonding can be observed in bulk IR spectra, indicated by the NH and CO stretch vibrations for **Cit-6** and **C8-6** at 3237 and 3262 cm^{-1} and 1636 and 1647 cm^{-1}, respectively (Table 1). Interestingly however, in MCH solutions, no triple helical hydrogen bonding can be observed in the IR spectrum, with the NH and CO stretch vibrations for **Cit-6** and **C8-6** at 3326 and 3318 cm^{-1} and 1663 and 1664 cm^{-1}, respectively, indicating a low degree of order in the hydrogen bonds (Table 2). The inability to form supramolecular polymers in solution is also reflected by the absence of a polymerization that is observable by VT-CD and VT-UV experiments (Fig. S15 and S17†).

Comparison of computational and experimental results

The results obtained from the bulk and solution state experiments confirm the trends of the different monomers that are observed in the MD simulations. Most notably, the MD simulations show that the central amides form hydrogen bonds with the ethers at the periphery, inducing kinks between ordered segments within the fibers. Interestingly, the number of defects appears to be regulated by a balance between the number and position of the ether moieties and the steric bulk at the periphery of the fibers.

The trends observed in the computational results rationalize the experimental data. **Cit-3** shows a relatively low number of amide–ether hydrogen bonds as well as a low number of persistent kinks throughout the simulation. This observation of a very ordered fiber is in line with the strong CD signal observed for this compound, as well as the high elongation temperature and cooperative self-assembly behavior. In addition, the IR spectra show that the amides form strong hydrogen bonds organized in a triple helical fashion in both bulk and MCH solutions, which corroborates the computational results.

The behavior of the dialkoxy-substituted benzyl-BTA derivatives is considerably different. The simulations of **Sym-Cit-6** show the highest number of amide–ether hydrogen bonds and the highest number of defects of all compounds simulated. Consequently, the ordered segments in these polymers are the shortest, in accordance with the complete absence of supramolecular polymers in solution or bulk in the conditions measured. The increased number of ether groups and their closer proximity to the central amides explain why the amide–ether hydrogen bonding can occur efficiently. Destabilization of the polymeric aggregates by these hydrogen bonds disrupts the integrity and stability of the polymer. As a result, **Sym-Cit-6** cannot form stable supramolecular polymers.

Surprisingly, the derivative that contains most ether moieties, **Cit-9**, shows only an intermediate amount of amide–ether hydrogen bonds in the simulations. The IR spectra of **Cit-9** in turn do not indicate that strong, helically organized hydrogen bonds are formed in either solution or bulk, as was observed for **Cit-3**. These results suggest that the moderate amounts of competitive hydrogen bonding of the amides with the ether groups may indeed interfere in the ordering of the supramolecular polymer. Despite the absence of helical hydrogen bonds, supramolecular polymers are present in solution, albeit with lower thermal stability and cooperativity than the polymers of **Cit-3**. The low degree of order in the supramolecular polymers is additionally reflected in the low CD intensity that these systems display. Nonetheless, the ability of **Cit-9** and **C8-9** to form polymers indicates that π-stacking also considerably contributes to the stability of the supramolecular polymers and that a balance between various hydrogen-bonding patterns and π-stacking determines the stability of the supramolecular polymers.

Together, the computational and experimental results show that amide–ether intermolecular hydrogen bonds, which compete with the amide–amide intermolecular hydrogen bonds, can significantly alter the stability and order of the supramolecular polymers. We propose that balancing these interactions may provide an avenue to tailor the stability and thermal properties in these non-covalent systems.

Conclusions

Despite the progress achieved in understanding the formation of supramolecular polymers, relationships between the molecular features of the monomers and stabilities of the

supramolecular polymers still remain elusive. To arrive at design rules for tunable stability in supramolecular polymerizations, insights gained from molecular simulations are to be combined with experimental studies. Here, we performed MD simulations on a series of tribenzyl-substituted benzene-1,3,5-carboxamide derivatives decorated with alkoxy-substituted benzyl moieties. The MD simulations show that, in comparison to the previously well studied trialkylbenzene-1,3,5-tricarboxamides (alkyl-BTAs), tris(alkoxybenzyl)benzene-1,3,5-tricarboxamides (benzyl-BTAs) organize in dynamic fibers with stacking defects such as kinks. These kinks appear and propagate at an extent and on a timescale that depend on the monomer structure.

Altogether, our results show that the degree of order along the fiber is a result of the competition between hydrogen bonding along the backbone of the supramolecular polymer with groups at the monomer periphery. The competition between these two hydrogen bonding patterns appears to be modulated by the steric demands of the peripheral alkyl substituents. The disordering effect due to amide–ether hydrogen bonds shown by the MD simulations was experimentally observed through differences of supramolecular polymerizations for the various compounds, both in the bulk and methylcyclohexane solutions. This combined approach is key to arrive at design principles and a complete understanding of supramolecular polymerizations. We hope our results will pave the way for such systematic studies of supramolecular polymers and other non-covalent systems both in water and organic media.

Conflicts of interest

There are no conflicts to declare.

Acknowledgements

MFJM and ARAP thank E.W. (Bert) Meijer for stimulating discussions, Elisabeth Weyandt for providing several aldehyde starting materials, and acknowledge financial support from NWO (TOP-PUNT Grant 10018944) and the Dutch Ministry of Education, Culture and Science (Gravitation program 024.001.035). RMR, HSC, JB and JMF acknowledge the Ministerio de Ciencia Innovación y Universidades (Spain) for funding through the Ramón y Cajal Program (RYC-2013-12570) and Proyectos I+D+i (CTQ2015-66869-P). HSC is grateful for a FPU fellowship from Ministerio de Educación Cultura y Deporte (Spain). The collaboration between Eindhoven and Mons is supported by the Fonds de la Recherche Scientifique – FNRS and the Fonds Wetenschappelijk Onderzoek under EOS Project No. 30650939. Computational resources have been provided by the Consortium des Équipements de Calcul Intensif (CÉCI), funded by the Fonds de la Recherche Scientifique de Belgique (F.R.S.-FNRS) under Grant No. 2.5020.11 and by the Wallonia Region. S. K., M. F. and M. S. thank Dr. Patrick Brocorens for helpful comments on the manuscript.

References

1 T. Aida, E. W. Meijer and S. I. Stupp, *Science*, 2012, **335**, 813–817.
2 L. Zang, Y. Che and J. S. Moore, *Acc. Chem. Res.*, 2008, **41**, 1596–1608.
3 S. S. Babu, V. K. Praveen and A. Ajayaghosh, *Chem. Rev.*, 2014, **114**, 1973–2129.
4 P. A. Korevaar, S. J. George, A. J. Markvoort, M. M. J. Smulders, P. A. J. Hilbers, A. P. H. J. Schenning, T. F. A. De Greef and E. W. Meijer, *Nature*, 2012, **481**, 492–496.
5 F. Fennel, S. Wolter, Z. Xie, P. A. Plötz, O. Kühn, F. Würthner and S. Lochbrunner, *J. Am. Chem. Soc.*, 2013, **135**, 18722–18725.
6 S. Ogi, C. Grzeszkiewicz and F. Würthner, *Chem. Sci.*, 2018, **9**, 2768–2773.
7 K. Cai, J. Xie, D. Zhang, W. Shi, Q. Yan and D. Zhao, *J. Am. Chem. Soc.*, 2018, **140**, 5764–5773.
8 A. Sorrenti, J. Leira-Iglesias, A. J. Markvoort, T. F. A. De Greef and T. M. Hermans, *Chem. Soc. Rev.*, 2017, **46**, 5476–5490.
9 S. Ogi, K. Sugiyasu, S. Manna, S. Samitsu and M. Takeuchi, *Nat. Chem.*, 2014, **6**, 188–195.
10 S. Ogi, T. Fukui, M. L. Jue, M. Takeuchi and K. Sugiyasu, *Angew. Chem., Int. Ed.*, 2014, **53**, 14363–14367.
11 J. Kang, D. Miyajima, T. Mori, Y. Inoue, Y. Itoh and T. Aida, *Science*, 2015, **347**, 646–651.
12 K. V. Rao, D. Miyajima, A. Nihonyanagi and T. Aida, *Nat. Chem.*, 2017, **9**, 1133–1139.
13 K. V. Rao, M. F. J. Mabesoone, D. Miyajima, A. Nihonyanagi, E. W. Meijer and T. Aida, *J. Am. Chem. Soc.*, 2020, **142**, 598–605.
14 M. Wehner, M. I. S. Röhr, M. Bühler, V. Stepanenko, W. Wagner and F. Würthner, *J. Am. Chem. Soc.*, 2019, **141**, 6092–6107.
15 J. S. Valera, R. Gómez and L. Sánchez, *Angew. Chem., Int. Ed.*, 2019, **58**, 510–514.
16 P. van der Schoot, in *Supramolecular Polymers*, 2nd edn, CRC Press, 2005.
17 R. Van Buel, D. Spitzer, C. M. Berac, P. Van Der Schoot, P. Besenius and S. Jabbari-Farouji, *J. Chem. Phys.*, 2019, **151**, 014902.
18 A. J. Markvoort, H. M. M. Ten Eikelder, P. A. J. Hilbers, T. F. A. De Greef and E. W. Meijer, *Nat. Commun.*, 2011, **2**, 509.
19 H. M. M. ten Eikelder, A. J. Markvoort, T. F. A. de Greef and P. A. J. Hilbers, *J. Phys. Chem. B*, 2012, **116**, 5291–5301.
20 H. M. M. ten Eikelder, B. Adelizzi, A. R. A. Palmans and A. J. Markvoort, *J. Phys. Chem. B*, 2019, **123**, 6627–6642.
21 J. Gershberg, F. Fennel, T. H. Rehm, S. Lochbrunner and F. Würthner, *Chem. Sci.*, 2016, **7**, 1729–1737.
22 Y. Liu, Y. Zhang, F. Fennel, W. Wagner, F. Würthner, Y. Chen and Z. Chen, *Chem. – Eur. J.*, 2018, **24**, 16388–16394.
23 M. Roman, C. Cannizzo, T. Pinault, B. Isare, B. Andrioletti, P. Van Der Schoot and L. Bouteiller, *J. Am. Chem. Soc.*, 2010, **132**, 16818–16824.
24 M. F. J. Mabesoone, A. J. Markvoort, M. Banno, T. Yamaguchi, F. Helmich, Y. Naito, E. Yashima, A. R. A.

Palmans and E. W. Meijer, *J. Am. Chem. Soc.*, 2018, **140**, 7810–7819.
25 K. K. Bejagam, G. Fiorin, M. L. Klein and S. Balasubramanian, *J. Phys. Chem. B*, 2014, **118**, 5218–5228.
26 K. K. Bejagam and S. Balasubramanian, *J. Phys. Chem. B*, 2015, **119**, 5738–5746.
27 A. Desmarchelier, M. Raynal, P. Brocorens, N. Vanthuyne and L. Bouteiller, *Chem. Commun.*, 2015, **51**, 7397–7400.
28 J. A. Berrocal, F. Di Meo, M. García-Iglesias, R. P. J. Gosens, E. W. Meijer, M. Linares and A. R. A. Palmans, *Chem. Commun.*, 2016, **52**, 10870–10873.
29 A. Desmarchelier, B. G. Alvarenga, X. Caumes, L. Dubreucq, C. Troufflard, M. Tessier, N. Vanthuyne, J. Idé, T. Maistriaux, D. Beljonne, P. Brocorens, R. Lazzaroni, M. Raynal and L. Bouteiller, *Soft Matter*, 2016, **12**, 7824–7838.
30 M. Garzoni, M. B. Baker, C. M. A. Leenders, I. K. Voets, L. Albertazzi, A. R. A. Palmans, E. W. Meijer and G. M. Pavan, *J. Am. Chem. Soc.*, 2016, **138**, 13985–13995.
31 P. W. J. M. Frederix, J. Idé, Y. Altay, G. Schaeffer, M. Surin, D. Beljonne, A. S. Bondarenko, T. L. C. Jansen, S. Otto and S. J. Marrink, *ACS Nano*, 2017, **11**, 7858–7868.
32 D. Bochicchio and G. M. Pavan, *ACS Nano*, 2017, **11**, 1000–1011.
33 P. Gasparotto, D. Bochicchio, M. Ceriotti and G. M. Pavan, *J. Phys. Chem. B*, 2020, **124**, 589–599.
34 C. Kulkarni, S. K. Reddy, S. J. George and S. Balasubramanian, *Chem. Phys. Lett.*, 2011, **515**, 226–230.
35 D. B. Korlepara, W. R. Henderson, R. K. Castellano and S. Balasubramanian, *Chem. Commun.*, 2019, **55**, 3773–3776.
36 Y. Nakano, T. Hirose, P. J. M. Stals, E. W. Meijer and A. R. A. Palmans, *Chem. Sci.*, 2012, **3**, 148–155.
37 J. J. Van Gorp, J. A. J. M. Vekemans and E. W. Meijer, *Mol. Cryst. Liq. Cryst.*, 2003, **397**, 191–205.
38 S. Ghosh, X.-Q. Li, V. Stepanenko and F. Würthner, *Chem. – Eur. J.*, 2008, **14**, 11343–11357.
39 R. van der Weegen, A. J. P. Teunissen, E. W. W. Meijer, R. Weegen and A. J. P. Teunissen, *Chem. – Eur. J.*, 2017, **23**, 1–12.
40 T. E. Kaiser, V. Stepanenko and F. Würthner, *J. Am. Chem. Soc.*, 2009, **131**, 6719–6732.
41 A. Sandeep, V. K. Praveen, D. S. Shankar Rao, S. Krishna Prasad and A. Ajayaghosh, *ACS Omega*, 2018, **3**, 4392–4399.
42 P. Kumar and M. Bansal, *J. Biomol. Struct. Dyn.*, 2012, **30**, 773–783.
43 Y. Matsunaga, N. Miyajima, Y. Nakayasu, S. Sakai and M. Yonenaga, *Bull. Chem. Soc. Jpn.*, 1988, **61**, 207–210.
44 P. J. M. Stals, M. M. J. Smulders, R. Martín-Rapún, A. R. A. Palmans and E. W. Meijer, *Chem. – Eur. J.*, 2009, **15**, 2071–2080.
45 C. Kulkarni, S. Balasubramanian and S. J. George, *ChemPhysChem*, 2013, **14**, 661–673.
46 C. Kulkarni, E. W. Meijer and A. R. A. Palmans, *Acc. Chem. Res.*, 2017, **50**, 1928–1936.
47 D. Zhao and J. S. Moore, *Org. Biomol. Chem.*, 2003, **1**, 3471–3491.
48 S. Kumar, *Handbook of liquid crystals*, Wiley-VCH Verlag, Weinheim, 2014.

